Environmental Science & Technology

Article

pubs.acs.org/est

Removing Arsenic from Synthetic Groundwater with Iron Electrocoagulation: An Fe and As K-Edge EXAFS Study

Case M. van Genuchten,[†,*] Susan E. A. Addy,[†] Jasquelin Peña,[‡,#] and Ashok J. Gadgil[†,§]

[†]Department of Civil and Environmental Engineering, University of California Berkeley, Berkeley, California 94720, United States

[‡]Earth Sciences Division, Lawrence Berkeley National Laboratory, Berkeley, California 94720, United States

[§]Environmental Energy Technologies Division, Lawrence Berkeley National Laboratory, Berkeley, California 94720, United States

Supporting Information

ABSTRACT: Electrocoagulation (EC) using iron electrodes is a promising arsenic removal strategy for Bangladesh groundwater drinking supplies. EC is based on the rapid in situ dissolution of a sacrificial Fe(0) anode to generate iron precipitates with a high arsenic sorption affinity. We used X-ray absorption spectroscopy (XAS) to investigate the local coordination environment (<4.0 Å) of Fe and As in EC precipitates generated in synthetic Bangladesh groundwater (SBGW). Fe and As K-edge EXAFS spectra were found to be similar between samples regardless of the large range of current density (0.02, 1.1, 5.0, 100 mA/cm^2) used to generate samples. Shell-by-shell fits of the Fe K-edge EXAFS spectra indicated that EC precipitates consist of primarily edge-sharing FeO_6 octahedra. The absence of corner-sharing FeO_6 octahedra implies that EC precipitates resemble nanoscale clusters (polymers) of edge-sharing octahedra that efficiently bind arsenic. Shell-by-shell fits of As K-edge EXAFS spectra show that arsenic, initially present as a mixture of As(III) and As(V), forms primarily binuclear, corner-sharing As(V) surface complexes on EC precipitates. This specific coordination geometry prevents the formation of FeO_6 corner-sharing linkages. Phosphate and silicate, abundant in SBGW, likely influence the structure of EC precipitates in a similar way by preventing FeO_6 corner-sharing linkages. This study provides a better understanding of the structure, reactivity, and colloidal stability of EC precipitates and the behavior of arsenic during EC. The results also offer useful constraints for predicting arsenic remobilization during the long-term disposal of EC sludge.

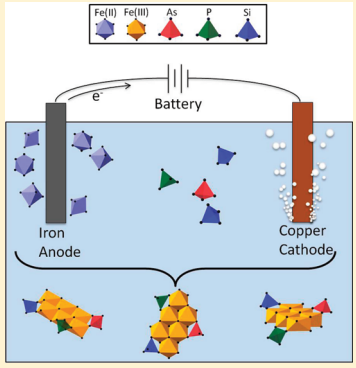

1. INTRODUCTION

Tens of millions of people worldwide are exposed to toxic concentrations of arsenic in groundwater drinking supplies, the vast majority living in rural Bangladesh.[1,2] A recent study estimates that 1 in 5 deaths in Bangladesh are due to arsenic exposure.[3] Despite much research during the past decade, the need for a sustainable solution to the arsenic crisis still exists. Electrocoagulation (EC) using Fe(0) electrodes is a promising arsenic removal strategy for Bangladesh because it is effective and low cost, produces minimal waste, and is easy to maintain and operate with locally available materials.[4−6]

EC is based on applying an electric current to a sacrificial Fe(0) anode to generate Fe ions. The Fe ions generated during EC polymerize rapidly, forming precipitates in situ with a high arsenic sorption affinity. The arsenic-laden precipitates can then be separated from treated water by gravitational settling and/or filtration. EC removes both As(III) and As(V) from wastewater and drinking water of varying pH and chemical characteristics.[5,7−9] However, the structures of EC precipitates generated in a Bangladesh groundwater matrix are not reported in prior literature.

The successful implementation of field-scale EC systems requires the optimization of operational parameters. The current density (current per unit area of electrode) of EC operation has been identified as a key parameter because it influences power consumption and treatment time.[4,5,10] Additionally, the current density may influence the structure of the generated Fe precipitate by altering the rate of Fe ion generation, which may lead to significant concentration gradients and local supersaturation with respect to different Fe (oxyhydr)oxide phases. Because the dominant mode of arsenic sorption varies among crystalline and amorphous Fe phases,[11] it is important to investigate the Fe precipitate structures over a wide range of practical current densities.

Previous studies indicate that the phase generated during EC is system-specific and may be influenced by the composition of the electrolyte (in addition to the current density). X-ray diffraction (XRD) has been used to detect Fe phases ranging from crystalline magnetite, maghemite, and lepidocrocite, to amorphous $FeAsO_4$ and hydrous ferric oxide (HFO) in different EC systems.[8,12−14] However, none of these studies characterized EC precipitates generated in an electrolyte similar in composition to groundwater of Bangladesh, which is rich in PO_4^{3-} and SiO_4^{4-}, with smaller concentrations of As(III) and As(V). The presence of PO_4^{3-}, SiO_4^{4-}, and AsO_4^{3-} has been

Received: June 4, 2011
Revised: August 25, 2011
Accepted: December 1, 2011
Published: December 1, 2011

 © 2011 American Chemical Society

reported to influence the structure of precipitates generated by Fe hydrolysis by reducing or preventing the formation of FeO_6 octahedral linkages.[15−17] Therefore, it is critical to study the Fe precipitate structure generated by EC in a groundwater matrix similar to the target region of Bangladesh with respect to major dissolved inorganic species.

Based on the work of Doeslch et al., Rose et al., and Waychunas et al.,[15−17] we expect that EC in a Bangladesh groundwater matrix will lead to poorly crystalline material that cannot be adequately characterized using XRD. Therefore, to best characterize the reaction products, we applied X-ray absorption spectroscopy (XAS) to determine the short-ranged structure of the precipitate and bonding structure of sorbed arsenic in EC precipitates generated in synthetic Bangladesh groundwater (SBGW) as a function of current density. The current density was varied over a larger range than in any other single previous EC study (5000 fold: 0.02−100 mA/cm^2) to investigate an extensive range of practical EC operating conditions. Knowledge of the local coordination about Fe should improve our understanding of the structure, reactivity, and colloidal stability of EC precipitates. An understanding of the dominant coordination geometry of arsenic (Figure 1) should provide insights into the behavior of arsenic during EC and offer useful constraints for predicting arsenic remobilization during the long-term disposal of EC sludge.

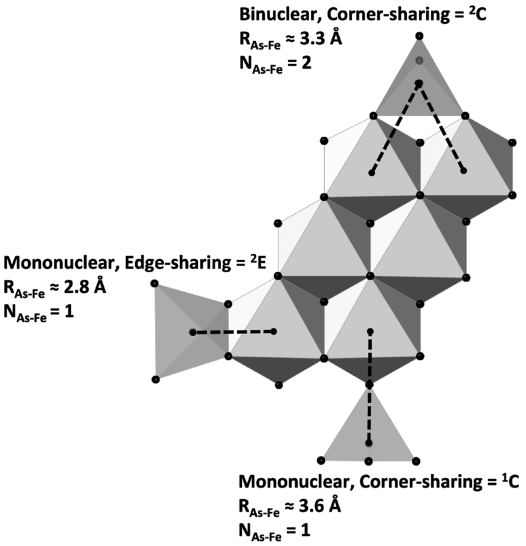

Figure 1. Possible inner-sphere coordination geometries of AsO_4 tetrahedra bound to a cluster of FeO_6 octahedra. N_{As-Fe} and R_{As-Fe} are given for each geometry.

2. MATERIALS AND METHODS

Synthetic Groundwater. The chemical composition of synthetic Bangladesh groundwater (SBGW; Table 1a) was derived from a comprehensive British Geological Survey (BGS) analysis of over 3500 tubewells from 61 of the 64 districts of Bangladesh.[18] Batches of SBGW were prepared with reagent-grade chemicals by first combining defined volumes of 4.0 mM $Na_2HAsO_4{\cdot}7H_2O$, 0.14 M $Na_2HPO_4{\cdot}7H_2O$, 0.45 M $NaHCO_3$, 0.84 mM $CaSO_4{\cdot}2H_2O$, 0.032 M $MgCl_2{\cdot}6H_2O$, and 0.14 M $CaCl_2$ stock solutions. After lowering pH < 6 by bubbling CO_2, silicate was introduced using a 0.070 M $Na_2SiO_3{\cdot}5H_2O$ stock solution under vigorous mixing to prevent silicate polymerization. To accurately represent groundwater of Bangladesh, the solution was purged with N_2 until pH increased to 7 and dissolved oxygen (DO) dropped below 2.0 mg/L. Finally, As(III) was introduced using a 4.0 mM $NaAsO_2$ stock solution. The conductivity of SBGW was determined to be approximately 990 μS/cm using an Accumet AP85 conductivity meter. Batches of SBGW were stored in a covered plastic carboy with N_2 continuously supplying the headspace until used in experiments. Batches were discarded unless used within 2 days of preparation.

EC Experimental Protocol. Experiments were conducted using an acid-washed Fe(0) wire anode coiled into a spiral and a Cu(0) mesh cathode spaced approximately 1 cm apart. Preliminary tests indicated that Pt(0) and Fe(0) cathodes behaved similarly to Cu(0), suggesting the cathode is likely inert in our EC system. The active area of the Fe(0) electrode was set by modifying the length of the submerged wire to produce the desired current density (J = 0.02, 1.1, 5.0, and 100 mA/cm^2). Current density (J [mA/cm^2]) is related to the charge loading (Q [C/L]), electrolysis time (t_e [s]), and electrode area to electrolyte volume ratio (A/V [cm^2/L]) through the relationship: $J = Q/[t_e{\cdot}(A/V)]$. To avoid excessive t_e values while investigating the 5000-fold variation in J, both A/V and t_e were varied during sample synthesis. The value of Q is related to the expected molar concentration of Fe generated during EC by Faraday's Law as follows: $Q/(n{\cdot}F)$ = [Fe], where n is the number of transferred electrons, and F is Faraday's constant (96485 C/mol). The calculation of Fe concentration assumes that n = 2 for the generation of Fe(II) from Fe(0).[19] A description of the operating parameters and relevant solids ratios for each sample is presented in Table 1b.

EC precipitates were synthesized by applying a galvanostatic current to the Fe(0) electrode in contact with SBGW (initial DO < 2.0 mg/L) under ambient atmospheric conditions. After the electrolysis stage, EC precipitates were continuously stirred and allowed to react with co-occurring ions for approximately 1 h. Solids were then separated from solution with a 0.1 μm filter. Concentrations of aqueous arsenic and iron in the clear filtrate were determined by inductively coupled plasma mass spectrometry (ICP-MS) performed by Curtis and Tompkins, Ltd. (Berkeley, CA) in experiments for which XAS samples were generated. In all other experiments, aqueous arsenic, iron, phosphate, and silicate were measured using a Perkin-Elmer 5300 DV inductively coupled plasma optical emission system

Table 1a. Solution Chemistry of SBGW[a]

Ion	Na^+ (mM)	Ca^{2+} (mM)	Mg^{2+} (mM)	Cl^- (mM)	HCO_3^- (mM)	SiO_4^{4-} (mM)	SO_4^{2-} (μM)	PO_4^{3-} (μM)	As(III) (μM)	As(V) (μM)	As(tot) μM	pH	Conductivity (μS/cm)
Initial	6.0	1.5	0.33	3.5	4.5	0.70	84	42	4.0	4.0	8.0	7.0	990
Post-treatment	–	–	–	–	–	0.50	–	1.0	–	–	0.10	7.4	930

[a]Post-treatment values are reported for J = 1.1 mA/cm^2. Removal fractions (1 − Post-treatment/Initial) of SiO_4^{4-}, PO_4^{3-} and As(tot) varied <5% across current densities. A dash (−) indicates unmeasured ions.

Table 1b. Sample Operating Parameters[a]

Sample	Spectra type	Current Density (mA/cm^2)	t_e (min)	Faradaic Fe Concentration (mM)	Si/Fe Solids Ratio (mmol/g)	P/Fe Solids Ratio (mmol/g)	As/Fe Solids Ratio (mmol/g)
J = 0.02	Fe K-edge	0.02	453	0.39	9.3	1.9	0.37
J = 1.1	Fe K-edge	1.1	25.6	0.91	4.0	0.82	0.16
J = 5.0	Fe K-edge	5.0	5.63	0.91	4.0	0.82	0.16
J = 100	Fe K-edge	100	3.17	0.91	4.0	0.82	0.16
J = 0.02	As K-edge	0.02	1170	0.39	9.3	1.9	0.37
J = 1.1	As K-edge	1.1	75.0	0.91	4.0	0.82	0.16
J = 5.0	As K-edge	5.0	16.3	0.91	4.0	0.82	0.16
J = 100	As K-edge	100	9.20	0.91	4.0	0.82	0.16

[a]A lower charge loading was used for the lowest current density samples (J = 0.02 mA/cm^2) because of the impractical t_e required to generate 175 C/L. The solids ratio was calculated using the amount of sorbate removed (mmol) divided by the Faradaic Fe mass (g).

(ICP-OES). In all experiments, Fe was undetectable in the filtrate.

X-ray Absorption Spectroscopy. A total of about 100 mg of solid was collected onto a filter membrane for each XAS measurement. The filter membranes were immediately transferred into a glovebox under N_2 atmosphere and taped to sample holders with kapton. Fe K-edge X-ray absorption spectra were collected at beamline 10.3.2 of the Advanced Light Source (ALS, Berkeley, CA) up to a reciprocal space value of 13.3 $Å^{-1}$ in transmission mode, calibrated to a Fe(0) foil (7110.75 eV). Beamline 10.3.2 was also used to acquire XRD patterns of representative samples (see Supporting Information (SI) for experimental details). Arsenic K-edge X-ray absorption spectra were collected at beamline 11-2 of the Stanford Synchrotron Radiation Laboratory (SSRL, Menlo Park, CA) up to a reciprocal space value of 14.3 $Å^{-1}$ in fluorescence mode, calibrated to an As(0) foil (11867 eV). The intensity of fluorescent X-rays was measured with a 30-element solid-state Ge detector (Canberra). Reference spectra for synthetic Fe (oxyhydr)oxides, including scorodite, magnetite, carbonate green rust, 2-line ferrihydrite (2LFH), and goethite, were provided by Dr. Peggy O'Day (University of California, Merced) and Dr. Brandy Toner (University of Minnesota) with sample preparation and data collection described previously by O'Day et al.[20] and Hansel et al.[21] A reference spectrum of As_2O_3 was obtained from a web-based library of model compounds.[22]

All data reduction and analyses were performed with SIXPack software.[23] Extended X-ray absorption fine structure (EXAFS) spectra were extracted from the deadtime-corrected, averaged, and normalized data, weighted by k^3, and Fourier transformed using a Kaiser-Bessel window with dk of 3.[24] Theoretical curve fitting was carried out in $R + \Delta R$-space (Å), based on algorithms derived from IFEFFIT.[25] Parameters varied in the fits included interatomic distance (R), coordination number (N), the mean squared atomic displacement (σ^2) and the change in threshold energy (ΔE_0). Theoretical phase and amplitude functions for single and multiple scattering paths were calculated using FEFF6.[26] Fe and As paths used in the fits were derived from the structures of goethite[27] and scorodite,[28] respectively. In the polyhedral approach, polymerization of individual FeO_6 octahedra into crystalline Fe phases occurs by corner-, edge-, and face-sharing octahedral linkages,[29,30] each with characteristic Fe−Fe interatomic distances distinguishable in the second-shell peak. In preliminary fits of the second-shell Fourier-transformed Fe and As K-edge EXAFS spectra, a high correlation between N and σ^2 led to high fit-determined errors. To eliminate these high correlations and high fit-determined errors, we followed the approach of Mikutta et al.,[31] and constrained the Fe second-shell fits by fixing σ^2 to the average of published values for Fe−Fe edge- and corner-sharing paths of similar Fe (oxyhydr)oxide precipitates (σ^2 = 0.012 $Å^2$, standard deviation = 0.004) [15,30−33] while allowing N to float. The As second-shell fits were carried out by floating σ^2 and fixing N_{As-Fe} to the value of the corresponding arsenic binding geometry (i.e., N_{As-Fe} is 1 and 2 for mononuclear and binuclear geometries, respectively). Sherman and Randall[34] suggested that the minimum value of the k-range used in the Fourier transform can influence the detection of different As surface complexes, including the ^2E complex. To avoid fitting artifacts originating from the Fourier transform window, two k-ranges were fit for each sample (3−13.5 and 4−13.5 $Å^{-1}$). Additional information regarding XAS sample preparation, data collection and analysis is provided in the SI.

3. RESULTS

Chemical Behavior in the EC Cell. During electrolysis, the clear and colorless electrolyte became turbid with a light orange color typical of Fe(III) (oxyhydr)oxides. Measurements of pH after electrolysis revealed a < 0.5 log unit increase, rather than the typical drop associated with Fe hydrolysis. Although HCO_3^- contributes to the pH buffering capacity of the solution, the evolution of $H_{2(g)}$ observed at the Cu(0) cathode can help balance the H^+ generated by the hydrolysis of Fe. For all but the lowest current density experiment (J = 0.02 mA/cm^2), DO decreased to <0.5 mg/L by the end of electrolysis and returned to at least its initial value (2.0 mg/L) after the mixing stage. Laboratory experiments at each current density (J = 0.02, 1.1, 5.0, and 100 mA/cm^2) showed more than 98, 94, and 25% removal of initial arsenic (8 μM), phosphate (42 μM) and silicate (0.70 mM) concentrations, respectively. In identical experiments to generate XAS samples, arsenic was similarly removed by more than 98% at each current density. Due to the removal of ions, the solution conductivity decreased to 930 μS/cm in each experiment.

Though a significant fraction of solids were filterable after the 1 h reaction time, the precipitates remained suspended over a 2−3 day period, indicating their colloidal stability. The X-ray diffractograms of EC precipitates (SI Figure S1) display features typical of nanocrystalline Fe(III) (oxyhydr)oxides such as 2-line ferrihydrite[32] with two broad peaks at d-spacings of approximately 1.50 and 2.57 Å. SEM images (SI Figure S2) of filtered solids revealed an aggregated particle size of approximately 50−200 nm composed of several smaller spherical subunits of approximately 10−30 nm.

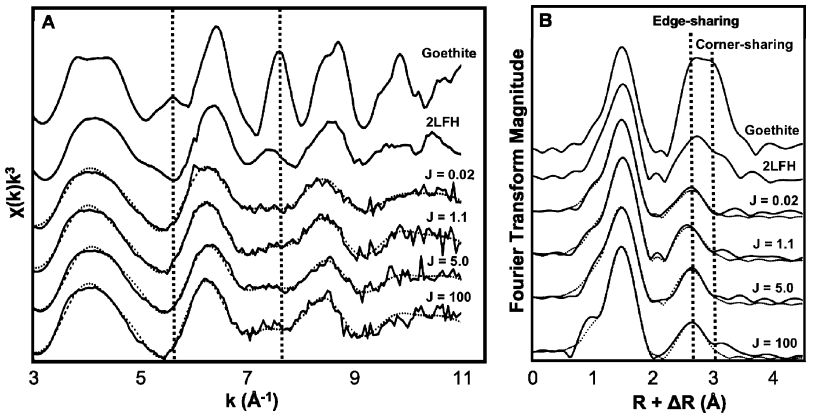

Figure 2. (a) Fe K-edge EXAFS spectra and (b) Fourier-transformed Fe K-edge EXAFS spectra (uncorrected for phase shift) of selected Fe reference materials and EC precipitates. The fits of EC precipitates (dashed lines) are superimposed on the data (solid black lines). The vertical lines in a) at approximately 5.7 and 7.4 $Å^{-1}$ indicate line shape features in goethite that arise from the presence of corner-sharing FeO_6 linkages and an increased number of edge-sharing FeO_6 octahedral linkages. These features are diminished in the EXAFS spectrum of 2LFH and disappear in the EXAFS spectra of EC precipitates. The vertical lines in (b) indicate peaks arising from edge-sharing and corner-sharing FeO_6 linkages.

Fe K-Edge X-ray Absorption Near Edge Structure (XANES). The Fe K-edge XANES spectra of EC precipitates were compared to those of Fe(II) and Fe(III) reference materials (SI Figure S3). The position of the absorption maximum of EC precipitates (7131.5 eV) is close to that of the Fe(III) reference materials, goethite and scorodite, indicating that Fe is present primarily as Fe(III). The absorption maximum of carbonate green rust (GR), a mixed valent Fe(II,III) (oxyhydr)oxide, clearly shifts to a lower X-ray energy due to the presence of Fe(II). The lack of an observable shoulder at lower energies in the XANES spectra of EC precipitates suggests that Fe(II) was not present at detectable levels. Lakshmanan et al.[19] have shown that only Fe(II) is generated in EC at current densities ranging from approximately 3−40 mA/cm^2. At high interface potentials, Fe(III) can be generated electrochemically during EC;[35] however, consistent with its decrease during electrolysis, DO is the most likely oxidant for Fe(II) in the EC system.

Fe K-Edge EXAFS. Figure 2a compares the Fe K-edge EXAFS spectra of EC precipitates to goethite and 2-line ferrihydrite, a nanocrystalline Fe phase. A change in the line shape of goethite compared to the other spectra is apparent between approximately 5.5 and 5.9 $Å^{-1}$. This peak is typical of crystalline Fe (oxyhydr)oxides and indicative of corner-sharing FeO_6 octahedra.[33] The EXAFS spectrum of goethite also shows a large peak at approximately 7.4 $Å^{-1}$. This spectral feature is dampened in 2-line ferrihydrite and disappears in the spectra of EC precipitates. The weakening of this feature arises from the loss of corner-sharing FeO_6 linkages and a decrease in the number of edge-sharing FeO_6 octahedral linkages.[33] Therefore, this feature indicates a progressive loss of structure from goethite to 2-line ferrihydrite to EC precipitates, with EC precipitates having less structural order than 2-line ferrihydrite. The spectra of EC precipitates, and to a lesser extent 2-line ferrihydrite, are dominated by broad, low amplitude oscillations at $k > 9$ $Å^{-1}$. The spectrum of goethite shows high amplitude oscillations throughout the analyzed k-range. Dampened spectral features at $k > 9$ $Å^{-1}$ are typical of the EXAFS spectra of HFO generated by Fe hydrolysis in the presence of strongly adsorbing organic and inorganic aqueous species.[15,16,32,33,36]

Shell-by-Shell Fits of the Fe K-Edge EXAFS Spectra. The magnitude of the Fourier transform (uncorrected for phase shift) of EC precipitates is compared to that of goethite and 2-line ferrihydrite in Figure 2b. Two peaks dominate the Fourier transform. The large peak located at approximately 1.5 Å ($R + \Delta R$) corresponds to the first shell of neighboring atoms within the FeO_6 octahedron. The second-shell peak arises from scattering from neighboring Fe atoms in the second coordination shell. The fits of EC precipitates are superimposed (dashed lines) on the data in Figure 2. Table 2a compares the results of the EC precipitate fits to those obtained by Toner et al.[33] for goethite and 2-line ferrihydrite.

Fe First-Shell Fits. The first shell of oxygen atoms of the FeO_6 octahedron was fit with one Fe−O path at approximately 1.98−1.99 Å. Fitting parameters (N_{Fe-O}, R_{Fe-O}, and σ^2) were similar among all of the EC precipitate samples. The somewhat large σ^2 value (0.009 $Å^2$) associated with the Fe−O path as compared to the Fe−O paths of goethite and 2-line ferrihydrite is likely due to the presence of multiple Fe−O distances within the FeO_6 octahedron. Although previous studies have reported the presence of two Fe−O distances of approximately 1.93 and 2.04 Å,[15,16,33] the spatial resolution of this data set ($\Delta R \approx \pi/(2\Delta k) \approx 0.2$) prevented fitting two Fe−O paths.[24] The fits produced N_{Fe-O} values near 6 for each sample, which is in agreement with the theoretical value if Fe atoms are in octahedral coordination.

Fe Second-Shell Fits. Only one Fe−Fe path at approximately 3.05−3.06 Å was required for the best fit of all EC precipitate samples. This path corresponds to FeO_6 octahedra sharing edges. The inclusion of additional Fe−Fe paths with distances of 3.26 and 3.43 Å yielded physically impossible N_{Fe-Fe} values and excessive (and often negative) values of σ^2 (i.e., $\sigma^2 = 0.19$ $Å^2$ for $J = 1.1$ mA/cm^2). In contrast, published fits of goethite and 2-line ferrihydrite required multiple Fe−Fe paths to fit both the edge-sharing and corner-sharing FeO_6 octahedral contributions at distances of 3.03 and 3.31 − 3.43 Å, respectively.[33] The lack of Fe−Fe scattering beyond approximately 3 Å in EC precipitates suggests that polyhedral linkages of longer distances, such as corner-sharing FeO_6 octahedra, were not present in detectable amounts. Although small differences in ΔE_0, R_{Fe-Fe}, and N_{Fe-Fe} exist among the samples, all parameters are in general agreement within the fit-derived uncertainties.

Table 2a. Summary of Fe Shell-by-shell Fitting Results

Sample	Atomic Pairs	N	R (Å)	σ^2 (Å^2)	ΔE_0 (eV)	R-Factor
J = 0.02	Fe−O	5.2 (0.5)	1.98 (0.01)	0.009 (0.001)	−4.2 (1.1)	0.014
	Fe−Fe	2.0 (0.3)	3.06 (0.01)	0.012		
J = 1.1	Fe−O	5.5 (0.4)	1.99 (0.01)	0.009 (0.001)	−3.6 (0.9)	0.010
	Fe−Fe	2.5 (0.3)	3.05 (0.01)	0.012		
J = 5.0	Fe−O	5.7 (0.5)	1.98 (0.01)	0.011 (0.001)	−2.9 (1.1)	0.016
	Fe−Fe	2.3 (0.3)	3.05 (0.01)	0.012		
J = 100	Fe−O	6.2 (0.6)	1.99 (0.01)	0.010 (0.001)	−3.6 (1.2)	0.018
	Fe−Fe	2.6 (0.4)	3.06 (0.01)	0.012		
2-line ferrihydrite	Fe−O1	2.7 (0.3)	1.92 (0.01)	0.003 (0.002)	1.3 (1.4)	0.010
	Fe−O2	N Fe−O1	2.04 (0.01)	0.005 (0.002)		
	Fe−Fe1	3.5 (1.7)	3.05 (0.02)	0.013 (0.004)		
	Fe−Fe2	1.4 (1.0)	3.45 (0.02)	0.006 (0.005)		
goethite	Fe−O1	3.0 (0.7)	1.95 (0.02)	0.003 (0.002)	2.6 (2.7)	0.020
	Fe−O2	N Fe−O1	2.09 (0.02)	0.005 (0.004)		
	Fe−Fe1	2.5	3.03 (0.01)	0.003 (0.001)		
	Fe−Fe2	N Fe−Fe1	3.31 (0.04)	0.004 (0.005)		
	Fe−Fe3	2N Fe−Fe1	3.44 (0.02)	0.006 (0.003)		

Table 2b. Summary of As Shell-by-Shell Fitting Results[a]

Sample	Atomic Pairs	N	R (Å)	σ^2 (Å^2)	ΔE_0 (eV)	R-factor
J = 0.02	As−O	4.2 (0.4)	1.69 (0.01)	0.002 (0.001)	7.6 (1.4)	0.030
	As−O−O	12	1.82(R_{As-O}) = 3.08	Sig (As−O)		
	As−Fe	2.0	3.24 (0.02)	0.007 (0.002)		
J = 1.1	As−O	4.2 (0.3)	1.70 (0.01)	0.002 (0.001)	8.3 (1.2)	0.022
	As−O−O	12	1.82(R_{As-O}) = 3.09	Sig (As−O)		
	As−Fe	2.0	3.27 (0.02)	0.010 (0.003)		
J = 5.0	As−O	4.0 (0.4)	1.70 (0.01)	0.003 (0.001)	7.4 (1.6)	0.040
	As−O−O	12	1.82(R_{As-O}) = 3.09	Sig (As−O)		
	As−Fe	2.0	3.26 (0.03)	0.010 (0.003)		
J = 100	As−O	4.0 (0.5)	1.70 (0.01)	0.003 (0.001)	7.4 (1.7)	0.043
	As−O−O	12	1.82(R_{As-O}) = 3.09	Sig (As−O)		
	As−Fe	2.0	3.26 (0.03)	0.010 (0.003)		

[a] N is the coordination number, R is the interatomic distance, σ^2 is the mean squared atomic displacement, ΔE_0 is the change in threshold energy. The passive electron reduction factor, S_0^2, was fixed at 0.6 and 0.95 for the fits of Fe and As respectively. Fitting parameters allowed to float are accompanied by fit-determined standard errors in parentheses. Constrained parameters appear without a parentheses. The k-range used in the Fourier transform was 3−11 Å^{-1} for Fe and 3−13.5 Å^{-1} for As. All fits were carried out from 1−4 Å in R + ΔR-space. The number of independent points (N_{idp}) for Fe and As were 15 and 17 respectively, whereas the number of variables (N_{var}) for both Fe and As was 6. The fitting results for 2-line ferrihydrite and goethite were taken from Toner et al.[33]

The Fourier-filtered spectra of EC precipitates provide further evidence that only a single Fe−Fe path contributes to the second shell. If multiple contributions were present in the second-shell peak, the filtered spectrum would show a characteristic "beat node",[24] as observed in the Fourier-filtered spectrum of goethite (SI Figure S4), and to a lesser extent 2-line ferrihydrite. No such beat node is evident in the Fourier-filtered second-shell peak of EC precipitates.

As K-Edge XANES. The As K-edge XANES spectra of EC precipitates were compared to those of As(III) and As(V) compounds (spectra shown in SI Figure S5). The shift in the absorption maximum of the reference compounds from 11872.4 to 11876.3 eV is consistent with an energy shift of approximately +2 eV per unit oxidation state previously reported for arsenic.[37] The maxima in the XANES spectra of EC precipitates at approximately 11876.5 eV are in agreement with the As(V) compound, $FeAsO_4$. Prior to electrolysis, the initial composition of SBGW consisted of equal concentrations of As(III) and As(V). The lack of a prominent shoulder in the XANES spectra of EC samples indicates oxidation of As(III) during treatment and that As(V) is the primary species present on EC precipitates.

As K-Edge EXAFS. Figure 3a shows the As K-edge EXAFS spectra of EC precipitates. The presence of similar peak positions and line-shapes among the EC samples suggest similar As coordination across all current densities. In each spectrum, the peaks of the first two oscillations at approximately 4.8 and 7.2 Å^{-1} are broadened compared to the peaks at approximately 9.7 and 12.0 Å^{-1}. A similar broadening in the first two oscillations was observed by Paktunc et al.[38] in the As K-edge EXAFS spectra of amorphous and crystalline $FeAsO_4$. Broadening of the first oscillation has been attributed to interference between the scattering of As−O and As−Fe atomic pairs, whereas broadening of the second oscillation arises from contributions of As−O−O multiple scattering within the AsO_4 tetrahedron.[38]

Shell-by-Shell Fits of the As K-Edge EXAFS Spectra. To determine the geometry of sorbed arsenic, theoretical curve fits were carried out to identify the specific atomic pair contributions to the first and second peaks. The fits of EC

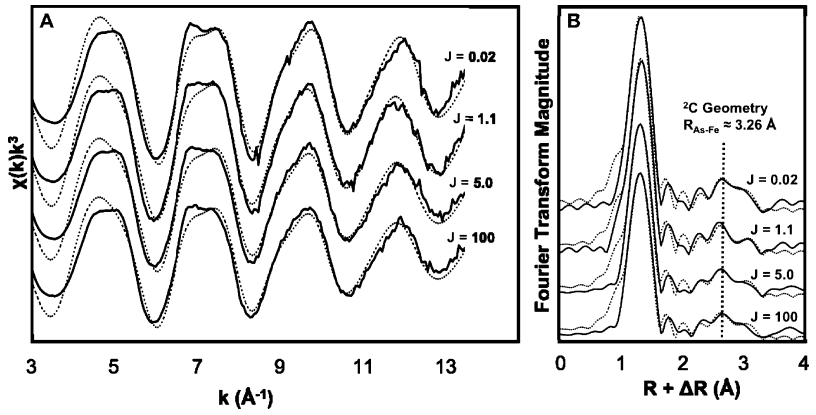

Figure 3. (a) As K-edge EXAFS spectra and (b) Fourier-transformed As K-edge EXAFS spectra (uncorrected for phase shift) of EC precipitates. The fits of EC precipitates (dashed lines) are superimposed on the data (solid black lines). The vertical line in (b) indicates the peak arising from arsenic bound in the binuclear ^2C geometry.

precipitates are superimposed (dashed lines) on the data in Figure 3. The results of the fits are given in Table 2b.

As First-Shell Fits. The values of R_{As-O}, N_{As-O}, and σ^2 determined by the fit of the first shell were similar among all EC precipitates and agreed within the standard error. N_{As-O} was found to be approximately 4.0−4.2 and R_{As-O} was approximately 1.69−1.70 Å, which is consistent with previous studies of tetrahedrally coordinated As(V) adsorbed to Fe (oxyhydr)oxides.[37,39] As(III) would have an N_{As-O} of approximately 3 and R_{As-O} of 1.78 Å.[11,40] The similarity of N_{As-O} and R_{As-O} with As(V) in tetrahedral coordination provides further evidence of the oxidation of As(III) to As(V) during EC treatment.

As−O−O Multiple Scattering Fits. Multiple scattering in highly symmetric polyhedra may be significant due to the high degeneracy of the scattering path. Since AsO_4 tetrahedra contain 12 As−O−O paths, an As−O−O path was added to the fit with constrained degeneracy of 12. Furthermore, in a regular tetrahedron, the distance between vertices is related to the distance from the center to a vertex by a geometrical factor. Thus, the value of R_{As-O-O} was constrained to be equal to the product of R_{As-O} and this geometrical factor $(^1/_2(2+(^8/_3))^{1/2})$. The value of R_{As-O-O} returned by the fit was 3.08 Å, which agrees closely with both theoretical and published values.[39] The addition of this multiple scattering As−O−O path improved the goodness-of-fit parameter, but did not affect the fit parameters obtained for the As−Fe second shell.

As Second-Shell Fits. Three possible geometries of As(V) bound to EC precipitates as inner-sphere surface complexes (Figure 1) can occur, each having a characteristic R_{As-Fe} value distinguishable in the second-shell peak of the Fourier-transformed EXAFS spectra. Mononuclear complexes sharing edges between AsO_4 and FeO_6 polyhedra (^2E) would have R_{As-Fe} values of approximately 2.8−2.9 Å.[17,41] AsO_4 tetrahedra bound in the binuclear ^2C geometry would bridge the oxygen atoms of adjacent FeO_6 octahedra and would have R_{As-Fe} values of approximately 3.2−3.3 Å.[17,41] Mononuclear complexes that share single corners between AsO_4 and FeO_6 polyhedra (^1C) would have an As−Fe distance of approximately 3.5−3.6 Å.[17,41]

For each sample at each analyzed k-range, the dominant geometry predicted by the fit was the ^2C configuration, based on R_{As-Fe} values of 3.26−3.27 Å (Figure 1). The addition of an As−Fe path corresponding to the ^2E geometry did not improve the fit by a statistically significant amount.[24] Moreover, σ^2 associated with the ^2E path was unreasonably large (σ^2 = 0.045 Å^2 for J = 1.1 mA/cm^2). The addition of an As−Fe path corresponding to the ^1C geometry or an As−As path corresponding to an AsO_4 polymer was not supported by our data using any k-range window for any sample. Finally, though previously observed on the surface of hematite,[42] an As(V) outer-sphere complex was not detectable in our data.

4. DISCUSSION

As(III) Oxidation. Both the absorption maxima in the As XANES spectra and the As−O interatomic distance determined from first-shell fits of the Fourier-transformed As K-edge EXAFS spectra indicate As(III) oxidation during EC treatment. A possible oxidant for As(III) in EC is Cl_2 generated by the anodic oxidation of Cl^- as hypothesized by Lakshmipathiraj et al.[13] However, the interface potential required to generate Cl_2 is likely higher than what would be available in this system. Dissolved oxygen can also oxidize As(III), but the reaction kinetics are too slow to contribute to As(III) oxidation in EC treatment.[43] The reactive intermediates generated during the oxidation of Fe(II) by DO[44] (i.e., Fenton-type reactions) likely play the largest role in the rapid As(III) oxidation seen here. Previous studies examining the Fe-catalyzed oxidation of As(III) in oxic systems have suggested the identity of the oxidant is pH-dependent, with the most likely oxidant being the ferryl ion (Fe(IV)) at near-neutral pH.[44] The slow and continuous addition and oxidation of Fe(II), rather than a one-time addition of an Fe(II) salt, has also been suggested as a way to maximize the efficiency and extent of Fe-catalyzed As(III) oxidation.[44,45] The ability to control the current density, and thus the supply of Fe(II) and reactive intermediates, in EC systems might be an advantage over the single addition of an Fe(II) salt. The oxidation of As(III) to As(V) can be beneficial in sorbent-based arsenic treatment systems because of the different sorption behavior of As(III) and As(V). At near-neutral pH, previous studies suggest that As(V) binds more strongly than As(III) to iron (oxyhydr)oxide mineral surfaces, making the removal of As(V) easier within this pH range.[46,47] The ^2C bonding structure derived from our EXAFS analysis is consistent with a strong As(V) inner-sphere complex.

Interaction of EC Precipitates with Arsenic and Co-Occurring Ions. Shell-by-shell fits of the Fourier-transformed Fe K-edge EXAFS spectra indicate that EC precipitates consist of primarily edge-sharing FeO_6 octahedra. The low degree of

FeO_6 polymerization can be explained by the high concentrations of oxyanions present in SBGW. Before treatment, SBGW contained considerable amounts of SiO_4^{4-} and PO_4^{3-}, with smaller concentrations of AsO_3^{3-} and AsO_4^{3-}. The substantial removal of AsO_4^{3-}, PO_4^{3-} and SiO_4^{4-} points to the strong affinity of these oxyanions for EC precipitate surfaces. The As shell-by-shell fits suggest that AsO_4 tetrahedra bind primarily in binuclear, corner-sharing complexes with the apical oxygen atoms of adjacent FeO_6 octahedra. Previous EXAFS studies have shown that SiO_4^{4-} and PO_4^{3-} likely bind in similar corner-sharing configurations to the same site as AsO_4^{3-} on Fe (oxyhydr)oxides.[15,16,48] This is the same site where free FeO_6 octahedra would join to form corner-sharing linkages. Sorption of oxyanions such as AsO_4^{3-}, PO_4^{3-} and SiO_4^{4-} can poison the surface of FeO_6 edge-sharing clusters and retard crystal growth by blocking the formation of FeO_6 corner-sharing linkages.[15−17,48] Moreover, corner-sharing FeO_6 octahedra are essential in the evolution from disordered FeO_6 polymers to crystalline (3-dimensional) Fe (oxyhydr)oxide phases. In SBGW, the high concentrations of PO_4^{3-} and SiO_4^{4-} are likely the cause of the nanocrystalline structure, with the lower concentration of AsO_4^{3-} playing a smaller role. The observed colloidal stability of the suspension (2−3 day settling time) is consistent with the nanoscale, surface-poisoned structure as determined by shell-by-shell fitting.

Due to the nanoscale structure of the EC precipitates, the insignificant contribution of the ^2E arsenic binding geometry is somewhat surprising. The ^2E and ^2C arsenic binding geometries on Fe (oxyhydr)oxide surfaces (Figure 1) are debated in the literature.[17,31,34,37,41] Short-ranged polymers consisting of only small clusters of edge-sharing FeO_6 octahedra should exhibit maximized edge-sharing sites.[36] Ample sites for the ^2E complex should be present in EC precipitates; however, the ^2C complex is the dominant geometry supported by the data. This may be due to the higher surface free energy of the ^2E geometry suggested by Sherman and Randall.[34]

Implications for Field Treatment. Since both the structure of EC precipitates and coordination geometry of sorbed arsenic were generally unchanged over a large range of current densities (0.02−100 mA/cm^2), the choice of optimum current density for EC operation will depend on trade-offs between additional operating parameters such as power consumption and treatment time. The applied voltage and power required to operate EC systems increase with increasing current density. However, the electrolysis time required to generate sufficient sorbent decreases with increasing current density. In rural areas with intermittent electricity, one might favor high power consumption (high current density) to complete treatment while power is available. Conversely, if the locality is connected to a reliable electrical grid, one might favor longer treatment duration (low current density) to minimize energy use.

The nanoscale structure of EC precipitates has implications for the application of EC as an arsenic removal technology. Nanoparticulate Fe (oxyhydr)oxides have a high surface area to volume ratio, which may lead to increased contaminant sorption per adsorbent mass.[49] The nanoparticulate clusters of FeO_6 octahedra identified in this study can reduce the electricity and mass of Fe needed for adequate arsenic removal due to their large specific surface area. However, separating colloidally stable FeO_6 clusters from treated water in this system might require additional steps. Improved separation can be achieved by adding a filter to treatment design or enhancing aggregation and settling by adding a coagulant, adjusting the background electrolyte concentration to the critical coagulation concentration (CCC), or adjusting the pH to the point of zero charge (PZC ∼ 8 for nanocrystalline iron (oxyhydr)oxides).[50] However, any additional step in treatment design may add complexity and unwanted supply chains to the system, which will be a burden on achieving low-cost, robust, and sustainable operation in the field.

The fate of arsenic and the likelihood of remobilization from EC precipitates after treatment is a concern for treatment efficiency and ultimate disposal of treatment sludge. Because As(V) forms multiple bonds to FeO_6 octahedra in the ^2C geometry, this inner-sphere surface complex will likely exhibit enhanced stability relative to the ^1C geometry or outer-sphere complex.[51] Evidence of the ^2C binuclear geometry as noted in our study is useful for explaining the minimal release of arsenic from Fe (oxyhydr)oxide precipitates reported in previous leaching tests.[52] Knowledge of the arsenic bonding structure determined in this study will also aid in the assessment of disposal strategies; however, a deeper understanding of the propensity of As(V) remobilization requires additional research.

■ ASSOCIATED CONTENT

Supporting Information

Detailed descriptions of XAS sample preparation, XAS and XRD data collection and reduction, SEM and XRD graphics, Fe and As XANES spectra, and the Fourier-filtered spectra of Fe reference material and EC precipitates. This material is available free of charge via the Internet at http://pubs.acs.org.

■ AUTHOR INFORMATION

Corresponding Author

*Phone: +1 (510) 664-4343; e-mail: cmvangenuchten@berkeley.edu.

Present Addresses

#Institut de Minéralogie et Géochimie Université de Lausanne Bâtiment Anthropole CH-1015 Lausanne

■ ACKNOWLEDGMENTS

We gratefully acknowledge support for this work by The Richard C. Blum Center for Developing Economies, a USEPA P3 Phase II award, The Sustainable Products and Solutions Program at Haas School of Business at UC Berkeley, and National Science Foundation Graduate Research Fellowship support to C.M.v.G. We are also thankful to Mathew Marcus, Sirine Fakra, John Bargar, Brandy Toner, Jonathan Slack, and Howdy Goudey for their generous advice and technical assistance at various stages of this work. Portions of this research were carried out at the Stanford Synchrotron Radiation Lightsource, a national user facility operated by Stanford University on behalf of the U.S. Department of Energy, Office of Basic Energy Sciences. The Advanced Light Source is a national user facility at LBNL, supported by the Director, Office of Science, Basic Energy Sciences, of the U.S. Department of Energy under Contract No. DE-AC02-05CH11231.

■ REFERENCES

(1) Singh, N.; Kumar, D.; Sahu, A. Arsenic in the environment: Effects on human health and possible prevention. *J. Environ. Biol.* **2007**, 359−365.

(2) Dhar, R.; Biswas, B.; Samanta, G.; Mandal, B.; Chakraborti, D.; Roy, S.; Jafar, A.; Islam, A.; Ara, G.; Kabir, S.; Khan, A.; Ahmed, S.; Hadi, S. Groundwater arsenic calamity in Bangladesh. *Curr. Sci.* **1997**, 48−59.

(3) Argos, M.; Kalra, T.; Rathouz, P.; Chen, Y.; Pierce, B.; Parvez, F.; Islam, T.; Ahmed, A.; Rakibuz-Zaman, M.; Hasan, R.; Sarwar, G.; Slavkovich, V.; van Geen, A.; Graziano, J.; Ahsan, H. Arsenic exposure from drinking water, and all-cause and chronic-disease mortalities in Bangladesh (HEALS): A prospective cohort study. *Lancet* **2010**, 252−258.
(4) Holt, P.; Barton, G.; Mitchell, C. The future for electrocoagulation as a localised water treatment technology. *Chemosphere* **2005**, 355−367.
(5) Kumar, P. R.; Chaudhari, S.; Khilar, K. C.; Mahajan, S. P. Removal of arsenic from water by electrocoagulation. *Chemosphere* **2004**, *55* (9), 1245−1252.
(6) Addy, S. E. A. Electrochemical Arsenic Remediation for Rural Bangladesh, Doctoral dissertation. University of California, Berkeley, Berkeley, 2008.
(7) Martinez-Villafane, J. F.; Montero-Ocampo, C.; Garcia-Lara, A. M. Energy and electrode consumption analysis of electrocoagulation for the removal of arsenic from underground water. *J. Hazard. Mater.* **2009**, *172* (2−3), 1617−1622.
(8) Wan, W.; Pepping, T. J.; Banerji, T.; Chaudhari, S.; Giammar, D. E., Effects of water chemistry on arsenic removal from drinking water by electrocoagulation. *Water Res.* **2010**, DOI: 10.1016/jwatres.2010.08.016.
(9) Lakshmanan, D.; Clifford, D.; Samanta, G. Comparative study of arsenic removal by iron using electrocoagulation and chemical coagulation. *Water Res.* **2010**, 5641−5652.
(10) Mollah, M. Y. A.; Morkovsky, P.; Gomes, J. A. G.; Kesmez, M.; Parga, J.; Cocke, D. L. Fundamentals, present and future perspectives of electrocoagulation. *J. Hazard. Mater.* **2004**, *114* (1−3), 199−210.
(11) Ona-Nguema, G.; Morin, G.; Juillot, F.; Calas, G.; Brown, G. E. EXAFS analysis of arsenite adsorption onto two-line ferrihydrite, hematite, goethite, and lepidocrocite. *Environ. Sci. Technol.* **2005**, *39* (23), 9147−9155.
(12) Gomes, J. A. G.; Daida, P.; Kesmez, M.; Weir, M.; Moreno, H.; Parga, J. R.; Irwin, G.; McWhinney, H.; Grady, T.; Peterson, E.; Cocke, D. L. Arsenic removal by electrocoagulation using combined Al-Fe electrode system and characterization of products. *J. Hazard. Mater.* **2007**, *139* (2), 220−231.
(13) Lakshmipathiraj, P.; Prabhakar, S.; Raju, G. B. Studies on the electrochemical decontamination of wastewater containing arsenic. *Sep. Purif. Technol.* **2010**, *73* (2), 114−121.
(14) Parga, P. A.; Vazquez, V.; Moreno, H., Thermodynamic studies of the arsenic adsorption on iron species generated by electrocoagulation. *J. Metall.* **2009**, *2009*, (Article ID 286971), 9 pages.
(15) Doelsch, E.; Rose, J.; Masion, A.; Bottero, J. Y.; Nahon, D.; Bertsch, P. M. Speciation and crystal chemistry of iron(III) chloride hydrolyzed in the presence of SiO4 ligands. 1. An Fe K-edge EXAFS study. *Langmuir* **2000**, *16* (10), 4726−4731.
(16) Rose, J.; Manceau, A.; Bottero, J. Y.; Masion, A.; Garcia, F. Nucleation and growth mechanisms of Fe oxyhydroxide in the presence of PO4 ions 0.1. Fe K-edge EXAFS study. *Langmuir* **1996**, *12* (26), 6701−6707.
(17) Waychunas, G. A.; Rea, B. A.; Fuller, C. C.; Davis, J. A. Surface-Chemistry of Ferrihydrite 0.1. Exafs Studies of the Geometry of Coprecipitated and Adsorbed Arsenate. *Geochim. Cosmochim. Acta* **1993**, *57* (10), 2251−2269.
(18) BGS *Arsenic Contamination of Groundwater in Bangladesh*; British Geological Survey: 2001.
(19) Lakshmanan, D.; Clifford, D. A.; Samanta, G. Ferrous and ferric ion generation during iron electrocoagulation. *Environ. Sci. Technol.* **2009**, *43* (10), 3853−3859.
(20) O'Day, P.; Rivera, N.; Root, R.; Carroll, S. X-ray absorption spectroscopic study of Fe reference compounds for the analysis of natural sediments. *Am. Mineral.* **2004**, 572−585.
(21) Hansel, C.; Benner, S.; Neiss, J.; Dohnalkova, A.; Kukkadapu, R.; Fendorf, S. Secondary mineralization pathways induced by dissimilatory iron reduction of ferrihydrite under advective flow. *Geochim. Cosmochim. Acta* **2003**, 2977−2992.
(22) Newville, M.; Carroll, S.; O'Day, P.; Waychunas, G.; Ebert, M. A web-based library of XAFS data on model compounds. *J. Synchrotron Radiat.* **1999**, 276−277.
(23) Webb, S. SIXPACK: A graphical user interface for XAS analysis using IFEFFIT. *Phys. Scr.* **2005**, *T115*, 1011−1014.
(24) Kelly, S. D.; Hesterberg, D.; Ravel, B. Analysis of soils and minerals using X-ray absorption spectroscopy. In *Methods of Soil Analysis. Part 5. Mineralogical Methods*, SSSA Book Series No. 5; Soil Science Society of America: Madison, WI2008.
(25) Newville, M. IFEFFIT: interactive XAFS analysis and FEFF fitting. *J. Synchrotron Radiat.* **2001**, 322−324.
(26) Rehr, J.; Albers, R.; Zabinsky, S. High-order multiple-scattering calculations of X-ray absorption fine structure. *Phys. Rev. Lett.* **1992**, 3397−3400.
(27) Gualtieri, A.; Venturelli, P. In situ study of the goethite-hematite phase transformation by real time synchrotron powder diffraction. *Am. Mineral.* **1999**, 895−904.
(28) Kitahama, K.; Kiriyama, R.; Baba, Y. Refinement of crystal-structure of scorodite. *Acta Crystallogr., Sect. B: Struct. Crystallogr. Cryst. Chem.* **1975**, 322−324.
(29) Manceau, A.; Combes, J. M. Structure of Mn and Fe Oxides and Oxyhydroxides - a Topological Approach by Exafs. *Phys. Chem. Miner.* **1988**, *15* (3), 283−295.
(30) Combes, J. M.; Manceau, A.; Calas, G.; Bottero, J. Y. Formation of ferric oxides from aqueous-solutions—A polyhedral approach by X-ray absorption-spectroscopy 0.1. Hydrolysis and formation of ferric gels. *Geochim. Cosmochim. Acta* **1989**, *53* (3), 583−594.
(31) Mikutta, C.; Frommer, J.; Voegelin, A.; Kaegi, R.; Kretzschmar, R. Effect of citrate on the local Fe coordination in ferrihydrite, arsenate binding, and ternary arsenate complex formation. *Geochim. Cosmochim. Acta* **2010**, 5574−5592.
(32) Voegelin, A.; Kaegi, R.; Frommer, J.; Vantelon, D.; Hug, S. J. Effect of phosphate, silicate, and Ca on Fe(III)-precipitates formed in aerated Fe(II)- and As(III)-containing water studied by X-ray absorption spectroscopy. *Geochim. Cosmochim. Acta* **2010**, *74* (1), 164−186.
(33) Toner, B. M.; Santelli, C. M.; Marcus, M. A.; Wirth, R.; Chan, C. S.; McCollom, T.; Bach, W.; Edwards, K. J. Biogenic iron oxyhydroxide formation at mid-ocean ridge hydrothermal vents: Juan de Fuca Ridge. *Geochim. Cosmochim. Acta* **2009**, *73* (2), 388−403.
(34) Sherman, D. M.; Randall, S. R. Surface complexation of arsenie(V) to iron(III) (hydr)oxides: Structural mechanism from ab initio molecular geometries and EXAFS spectroscopy. *Geochim. Cosmochim. Acta* **2003**, *67* (22), 4223−4230.
(35) Bard, A. J.; Faulkner, L. R., *Electrochemical Methods: Fundamentals and Applications*, 2nd ed.; Wiley: New York, 2001; p xxi.
(36) Waychunas, G. A.; Davis, J. A.; Fuller, C. C. Geometry of sorbed arsenate on ferrihydrite and crystalline Feooh—Reevaluation of exafs results and topological factors in predicting sorbate geometry, and evidence for monodentate complexes. *Geochim. Cosmochim. Acta* **1995**, *59* (17), 3655−3661.
(37) Manning, B. A.; Hunt, M. L.; Amrhein, C.; Yarmoff, J. A. Arsenic(III) and arsenic(V) reactions with zerovalent iron corrosion products. *Environ. Sci. Technol.* **2002**, *36* (24), 5455−5461.
(38) Paktunc, D.; Dutrizac, J.; Gertsman, V. Synthesis and phase transformations involving scorodite, ferric arsenate and arsenical ferrihydrite: Implications for arsenic mobility. *Geochim. Cosmochim. Acta* **2008**, 2649−2672.
(39) Morin, G.; Ona-Nguema, G.; Wang, Y. H.; Menguy, N.; Juillot, F.; Proux, O.; Guyot, F.; Calas, G.; Brown, G. E. Extended X-ray absorption fine structure analysis of arsenite and arsenate adsorption on maghemite. *Environ. Sci. Technol.* **2008**, *42* (7), 2361−2366.
(40) Thoral, S.; Rose, J.; Garnier, J. M.; Van Geen, A.; Refait, P.; Traverse, A.; Fonda, E.; Nahon, D.; Bottero, J. Y. XAS study of iron and arsenic speciation during Fe(II) oxidation in the presence of As(III). *Environ. Sci. Technol.* **2005**, *39* (24), 9478−9485.
(41) Manceau, A. The mechanism of anion adsorption on iron-oxides— Evidence for the bonding of arsenate tetrahedra on free

Fe(O,Oh)(6) edges. *Geochim. Cosmochim. Acta* **1995**, *59* (17), 3647–3653.
(42) Catalano, J.; Park, C.; Fenter, P.; Zhang, Z. Simultaneous inner- and outer-sphere arsenate adsorption on corundum and hematite. *Geochim. Cosmochim. Acta* **2008**, *72* (8), 1986–2004.
(43) Lowry, J. D.; Lowry, S. B. *Oxidation of As(III) by Aeration and Storage*; NRML Office of Research and Development, U.S. EPA: Cincinnati, OH, 2002.
(44) Hug, S. J.; Leupin, O. Iron-catalyzed oxidation of arsenic(III) by oxygen and by hydrogen peroxide: pH-dependent formation of oxidants in the Fenton reaction. *Environ. Sci. Technol.* **2003**, *37* (12), 2734–2742.
(45) Bisceglia, K.; Rader, K.; Carbonaro, R.; Farley, K.; Mahony, J.; Di Toro, D. Iron(II)-catalyzed oxidation of arsenic(III) in a sediment column. *Environ. Sci. Technol.* **2005**, 9217–9222.
(46) Dixit, S.; Hering, J. G. Comparison of arsenic(V) and arsenic(III) sorption onto iron oxide minerals: Implications for arsenic mobility. *Environ. Sci. Technol.* **2003**, *37* (18), 4182–4189.
(47) Raven, K. P.; Jain, A.; Loeppert, R. H. Arsenite and arsenate adsorption on ferrihydrite: Kinetics, equilibrium, and adsorption envelopes. *Environ. Sci. Technol.* **1998**, *32* (3), 344–349.
(48) Rose, J.; Flank, A. M.; Masion, A.; Bottero, J. Y.; Elmerich, P. Nucleation and growth mechanisms of Fe oxyhydroxide in the presence of PO4 ions 0.2. P K-edge EXAFS study. *Langmuir* **1997**, *13* (6), 1827–1834.
(49) Waychunas, G.; Kim, C.; Banfield, J. Nanoparticulate iron oxide minerals in soils and sediments: Unique properties and contaminant scavenging mechanisms. *J. Nanopart. Res.* **2005**, 409–433.
(50) Stumm, W.; Sigg, L.; Sulzberger, B., *Chemistry of the Solid-Water Interface: Processes at the Mineral-Water and Particle-Water Interface in Natural Systems*; Wiley: New York, 1992; p x.
(51) Brown, G.; Foster, A.; Ostergren, J. Mineral surfaces and bioavailability of heavy metals: A molecular-scale perspective. *Proc. Natl. Acad. Sci. U.S.A.* **1999**, *96* (7), 3388–3395.
(52) Ghosh, A.; Mukiibi, M.; Ela, W. TCLP underestimates leaching of arsenic from solid residuals under landfill conditions. *Environ. Sci. Technol.* **2004**, 4677–4682.